Journal Pre-proofs

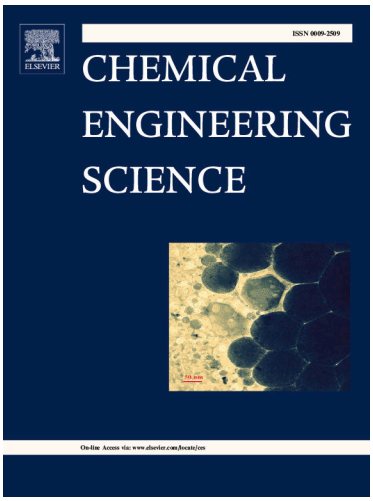

Recovery of rare earth elements, gallium and germanium from fly ash and red mud via ultra-fast flash Joule heating

Zhe Sun, Zuimiao Tao, Heyu Li, Aaron S Pittman, Faxing Zhou, Gengmin Zhang, Junchi Wu, Hong Cheng, Enlang Feng, Zhennan Chen, Yan Cao

PII: S0009-2509(25)00702-X
DOI: https://doi.org/10.1016/j.ces.2025.121879
Reference: CES 121879

To appear in: *Chemical Engineering Science*

Received Date: 17 February 2025
Revised Date: 9 May 2025
Accepted Date: 17 May 2025

Please cite this article as: Z. Sun, Z. Tao, H. Li, A.S. Pittman, F. Zhou, G. Zhang, J. Wu, H. Cheng, E. Feng, Z. Chen, Y. Cao, Recovery of rare earth elements, gallium and germanium from fly ash and red mud via ultra-fast flash Joule heating, *Chemical Engineering Science* (2025), doi: https://doi.org/10.1016/j.ces.2025.121879

Recovery of Rare Earth Elements, Gallium and Germanium from Fly Ash and Red Mud via Ultra-fast Flash Joule Heating

Zhe Sun[a,b,c,d], Zuimiao Tao[b,c,d], Heyu Li[b,c,d], Aaron S Pittman[b,c,d,e], Faxing Zhou[f], Gengmin Zhang[f], Junchi Wu[g], Hong Cheng[g], Enlang Feng[h], Zhennan Chen[h], Yan Cao[a,b,c,d,e,f,g,h,*]

[a] AnHui Province Key Laboratory of Chemistry for Inorganic/Organic Hybrid Functionalized Materials, Anhui University, Hefei, 230601, China

[b] Guangzhou Institute of Energy Conversion, Chinese Academy of Sciences, Guangzhou 510640, China

[c] CAS Key Laboratory of Renewable Energy, Guangzhou 510640, China

[d] Guangdong Provincial Key Laboratory of Renewable Energy, Guangzhou 510640, China

[e] School of Energy Science and Engineering, University of Science and Technology of China, Guangzhou 510640, China.

[f] Guangxi Investment Group Lingang Industrial Co., Ltd, Beihai 536000, China

[g] Guangxi Huayin Aluminum Industry Co., Ltd, Baise 533700, China

[h] Geely Baikuang Group Research Aluminum Industry Research Institute, Baise 533700, China.

[*] Corresponding author. E-mail address: caoyan@ms.giec.ac.cn

Abstract

The substantial quantities of fly ash and red mud generated and contains abundant rare earth elements, gallium, and germanium. Their effective recovery not only mitigates environmental impacts but also unlocks significant economic benefits. This work developed an ultra-fast flash Joule heating activation coupled with acid leaching method to recover rare earth elements, gallium, and germanium from fly ash and red mud. By leveraging ultra-fast flash Joule heating, the approach recreates the silicon-aluminium crystal phases in red mud and fly ash under instantaneous, extreme high-

temperature conditions (2000–3000°C), achieving an acid leaching recovery efficiency exceeding 80% for rare earths, gallium, and germanium. In contrast to conventional pyrometallurgical methods (such as alkali treatment activation followed by water/alkali washing and acid leaching) this instantaneous ultra-high-temperature Joule heating process enables efficient rare earth, gallium, and germanium extraction without alkali addition, demonstrating low energy and acid consumption.

Keywords: Resource recovery, Rare earth elements, Gallium, Germanium, Flash Joule Heating

1. Introduction

Rare earth elements (REEs) , gallium (Ga), and germanium (Ge) are recognized as strategic critical minerals [1-3], pivotal to modern high-tech industries. Owing to their unique magnetic, optical, and electrical properties, REEs are extensively applied across aerospace, information technology, electronics, energy, transportation, and medical sectors. Ga and Ge serve as key components in third- and fourth-generation advanced semiconductor materials, indispensable for manufacturing high-performance chips and other cutting-edge electronic devices. Concurrently, global demand for these elements has been steadily rising, driven by technological advancements and emerging green energy applications. However, economic and environmental challenges, coupled with licensing complexities and trade restrictions, have heightened international concerns regarding the security and sustainability of their supply chains.

In 2023, over 899 million tons of fly ash [4] and 107 million tons of red mud [5] were generated in China. Current management practices for fly ash and red mud primarily involve open-air stacking and landfilling, with their comprehensive utilization rates remaining suboptimal. The massive accumulation of these byproducts not only occupies substantial land and resources, hindering industrial productivity, but also exacerbates environmental pollution through leaching and dust emissions. Notably, fly ash and red mud exhibit anomalous enrichment of co-occurring REEs, Ga, and Ge, making their secondary recovery a critical supplementary source for mineral extraction, especially amid rising demand and escalating challenges in primary ore mining for these strategic elements [6-11]. However REEs, Ga, and Ge in fly ash and red mud are tightly encapsulated within silico-aluminum crystalline phases, rendering direct acid leaching ineffective for efficient recovery. Previous studies by Lin et al. [10], Pan et al. [12], Heileen et al. [13], and Mokoena et al. [14] have demonstrated that alkali fluxes (such as Na_2CO_3, Na_2O_2, NaOH, and KOH) can enhance REEs extraction via alkali melting, achieving recovery rates of up to 90%. Despite these advancements, existing recovery technologies for these elements suffer from inherent drawbacks: lengthy

processing times, excessive material/energy consumption, and high carbon emissions, challenges that remain unaddressed in current methodologies. Consequently, developing a viable recovery method requires overcoming these four key bottlenecks to improve resource utilization efficiency and establish a sustainable extraction mechanism.

Ultra-fast flash Joule heating (FJH) technology, an emerging solid waste treatment methodology, leverages capacitive discharge to instantaneously release a massive electrical charge, generating transient high temperatures (up to 3000℃) within the reactor for material processing. This technology has garnered significant attention in the field of solid waste valorization. Through precise control of ultra-high-temperature heating and rapid cooling, it enables effective treatment of diverse waste streams: inorganic matrices like fly ash and contaminated soil, as well as complex mixtures such as electronic waste and spent batteries, thereby facilitating resource recovery and value-added utilization. Tour et al.[15], Paul et al. [16] and Wyss et al. [17] achieved the preparation of graphene and carbon nanotubes from carbon-containing solid waste using the ultra-fast FJH technology. Yun et al.[18], Guo et al. [19], and Chen et al. [20] have treated a large amount of discarded lithium-ion batteries using the ultra-fast FJH technology, achieving the regeneration and utilization of waste lithium-ion batteries. Chen et al. [21] and Zhu et al.[22] efficiently recovered metal ions such as Li, Co, and Ni from electrodes using the ultrafast FJH technology. Deng et al. [23] removed heavy metals such as Cd, As, Pb, Co, Ni, and other metals from fly ash.

Based on the characteristics of ultra-fast FJH technology, this study pioneers the application of FJH for recovering REEs, Ga, and Ge from fly ash and red mud. Breaking through the constraints of prolonged thermal treatment in conventional methods, the research successfully reconstructed silicon-aluminum crystalline phases in these solid wastes under FJH-induced subsecond-scale instantaneous ultrahigh temperature condition. A novel process, ultra-fast FJH activation coupled with acid leaching, is designed to extract REEs, Ga, and Ge from fly ash and red mud. In contrast to the alkali-fusion alkali-leaching methods of calcination alkali activation, water washing, alkali washing, and acid leaching, the efficient extraction of REEs, Ga, and Ge was achieved with short time, low material consumption, low energy consumption, and low carbon emissions, offering a novel approach for the extraction of REEs, Ga, and Ge from fly ash and red mud.

2. Materials and Methods

2.1 Fly ash and red mud samples

The fly ash and red mud were collected from coal-fired power plants of domestic coal enterprises and alumina refineries of aluminum enterprises. The major elements

were characterized using X-ray fluorescence spectroscopy (XRF), and REEs, Ga, and Ge were analyzed using inductively coupled plasma mass spectrometry (ICP-MS). Table 1 shows the characterization data. In fly ash, Al_2O_3 and SiO_2 constituted the dominant components (83.50% in total), followed by Fe_2O_3 (2.92%). Conversely, red mud was primarily composed of Fe_2O_3 (57.23%) with Al_2O_3 and SiO_2 accounting for a combined 27.23%. REEs analysis showed that fly ash and red mud samples contained 457.23 μg/g and 310.22 μg/g of REEs, respectively, with light-to-heavy REE ratios of 2.97 and 2.53 for light and heavy REEs, indicating significant enrichment of heavy REEs, a critical feature for industrial value. Ga concentrations were 72.69 μg/g (fly ash) and 103.00 μg/g (red mud), while Ge measured 11.10 μg/g and 35.12 μg/g, respectively. Based on annual production volumes of 10 million tons (fly ash) and 3 million tons (red mud) by the studied enterprises, estimated annual reserves include ~4,500 tons and ~930 tons of REEs, ~700 tons and ~300 tons of Ga, and ~110 tons and ~105 tons of Ge, respectively, highlighting the substantial economic potential of these waste streams.

Table 1. Characterization of the fly ash (FA) and red mud (RM)

Major Elements (%)			**REES (μg/g)**				
	FA	RM		FA	RM		FA	RM
Na_2O	0.66	5.00	La	78.17	53.81	Dy	9.80	4.27
MgO	0.40	0.26	Ce	151.26	110.80	Ho	2.00	1.26
Al_2O_3	27.70	21.85	Pr	17.24	10.08	Er	5.74	3.68
SiO_2	55.80	5.38	Nd	64.77	34.04	Tm	0.82	0.52
K_2O	1.23	0.41	Sm	12.10	5.71	Yb	5.27	2.66
CaO	0.88	3.19	Eu	2.58	1.65	Lu	0.82	0.22
Fe_2O_3	2.92	57.23	Gd	12.24	5.20	Sc	33.37	47.38

Ga & Ge (μg/g)			Tb	3.68	0.98	3.68	0.98	27.95
	FA	RM	LREE	342.04	222.27	HREE	115.19	87.95
Ga	72.69	103.00	∑REE	457.23	310.22			
Ge	11.10	35.12	L/H	2.97	2.53			

2.2 Reagents used in the experiment

All reagents used in the experiment were analytical grade, and the conductivity of the pure water had a conductivity of ≥ 18MΩ· cm. Specifically, ammonium acetate and hydrofluoric acid were supplied by Macklin (Shanghai Macklin Biochemical Technology Co., Ltd.). Hydrochloric acid, sodium carbonate, hydrogen peroxide, and anhydrous ethanol were all produced from Sinopharm Chemical Reagent Co., Ltd, while graphite powder was manufactured by Tianjin Dengke Chemical Reagent Co., Ltd.

2.3 Ultra-fast FJH system

The ultra-fast FJH system comprises two core components: a charge-discharge test chamber and a flash reaction chamber. The charge-discharge test chamber serves as the primary electrical unit, integrating a direct current (DC) power supply, voltmeter, capacitor, charging circuit breaker, arc-quenching circuit breaker, discharge circuit breaker, insulated gate bipolar transistor (IGBT) module with driver, and power resistor. The flash reaction chamber, designed to maintain vacuum or controlled atmospheric conditions for FJH reactions, includes a sealed reaction vessel, tubular reaction apparatus, vacuum pump, infrared temperature sensor, and auxiliary components.

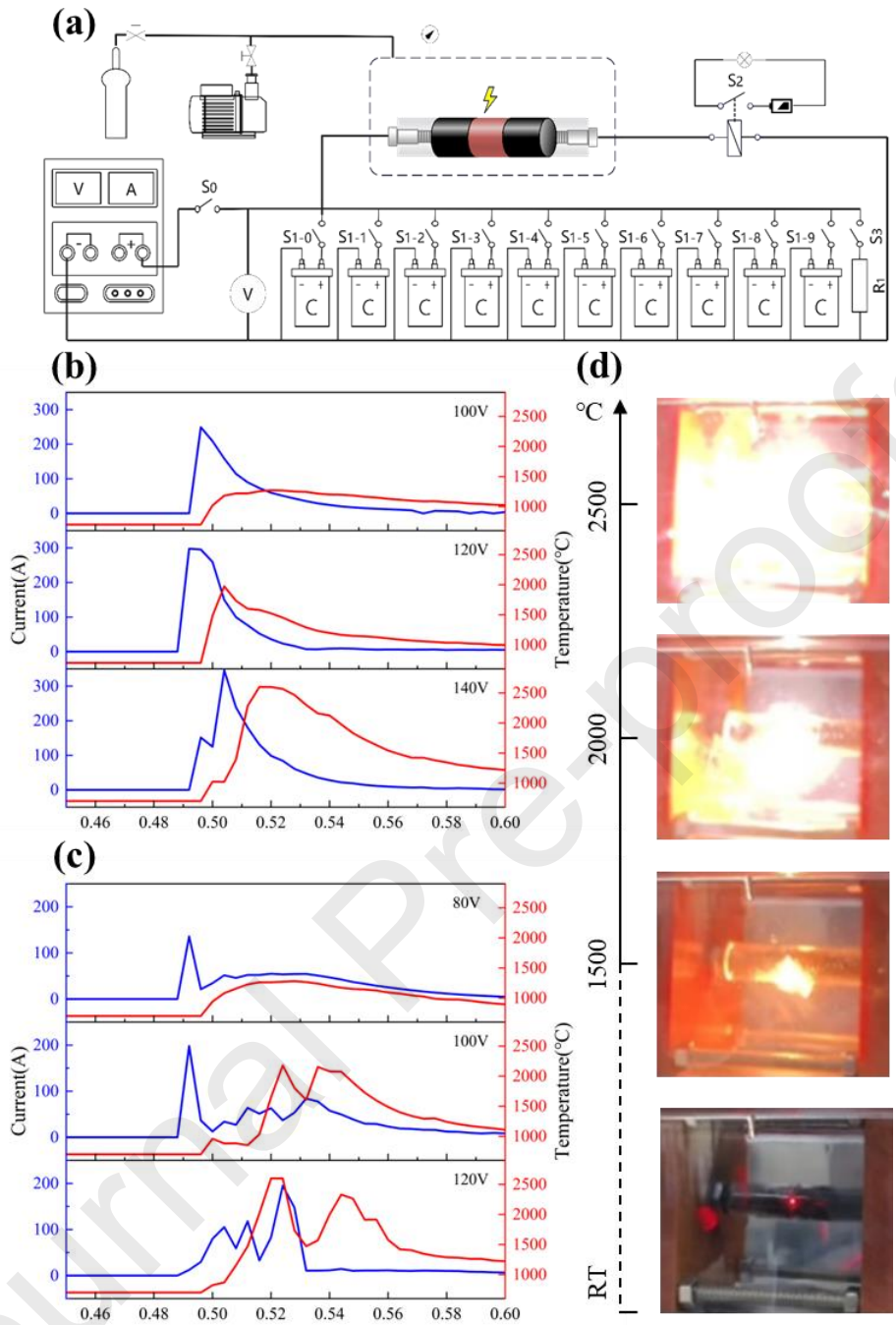

Figure 1. (a) Schematic of the ultra-fast FJH device; (b) & (c) temperature-time and current-time profiles for flash heating activation of fly ash and red mud at varying voltages; (d) photographic record of the fly ash activation process at 140 V

The ultra-fast FJH activation experiment entailed mixing fly ash or red mud samples with graphite powder at a 2:1 mass ratio as a conductive additive. A 100 mg portion of the mixture was loaded into a quartz tube, which was then integrated into the equipment's charge-discharge test chamber for FJH treatment. The schematic of the

ultra-fast FJH system is shown in Figure 1a. Electrode pressure was adjusted to control sample resistance, which was maintained at 1Ω for most experiments. Extreme resistance values (both high and low) compromised FJH performance: high resistance restricted current supply, while low resistance caused heat dissipation to the electrodes rather than the sample, both preventing sufficient heating. Discharge behaviors of fly ash and red mud under varying voltages (within 0.2 seconds of discharge time) are shown in Figures 1b and 1c, respectively. As voltage increased, the current through the sample rose proportionally, leading to a corresponding temperature rise. The maximum recorded currents were 350 A (fly ash) and 200 A (red mud), respectively. The ultra-fast FJH system achieved sample temperatures up to 2600℃ within 0.1 seconds, a critical condition for disrupting the silico-aluminum crystalline structure in the samples. The relatively stable current profile of fly ash stemmed from its rigid silico-aluminum framework, whereas red mud's current fluctuations were attributed to resistance changes during degassing or rapid heating.

2.5 Sequential Chemical Extraction Speciation Methodology

The occurrence states of REEs, Ga, and Ge in fly ash and red mud are categorized into five fractions: water-soluble form (WSF), ion-exchangeable form (IEF), acid-soluble form (ASF), sulfided form (SF), and residual form (RF). A sequential chemical extraction method was employed to distinguish these distinct speciation states, thereby facilitating the gradual revelation of trace element distributions within the samples. This approach serves as a powerful analytical tool for in-depth investigations into the potential utilization of REEs, Ga, Ge, and other trace element resources. Notably, this extraction method and analytical approach can be effectively applied not only to the current experiment but also to pedagogical practices in related experimental courses. The detailed extraction procedure is outlined in Figure 2 and Table 2.

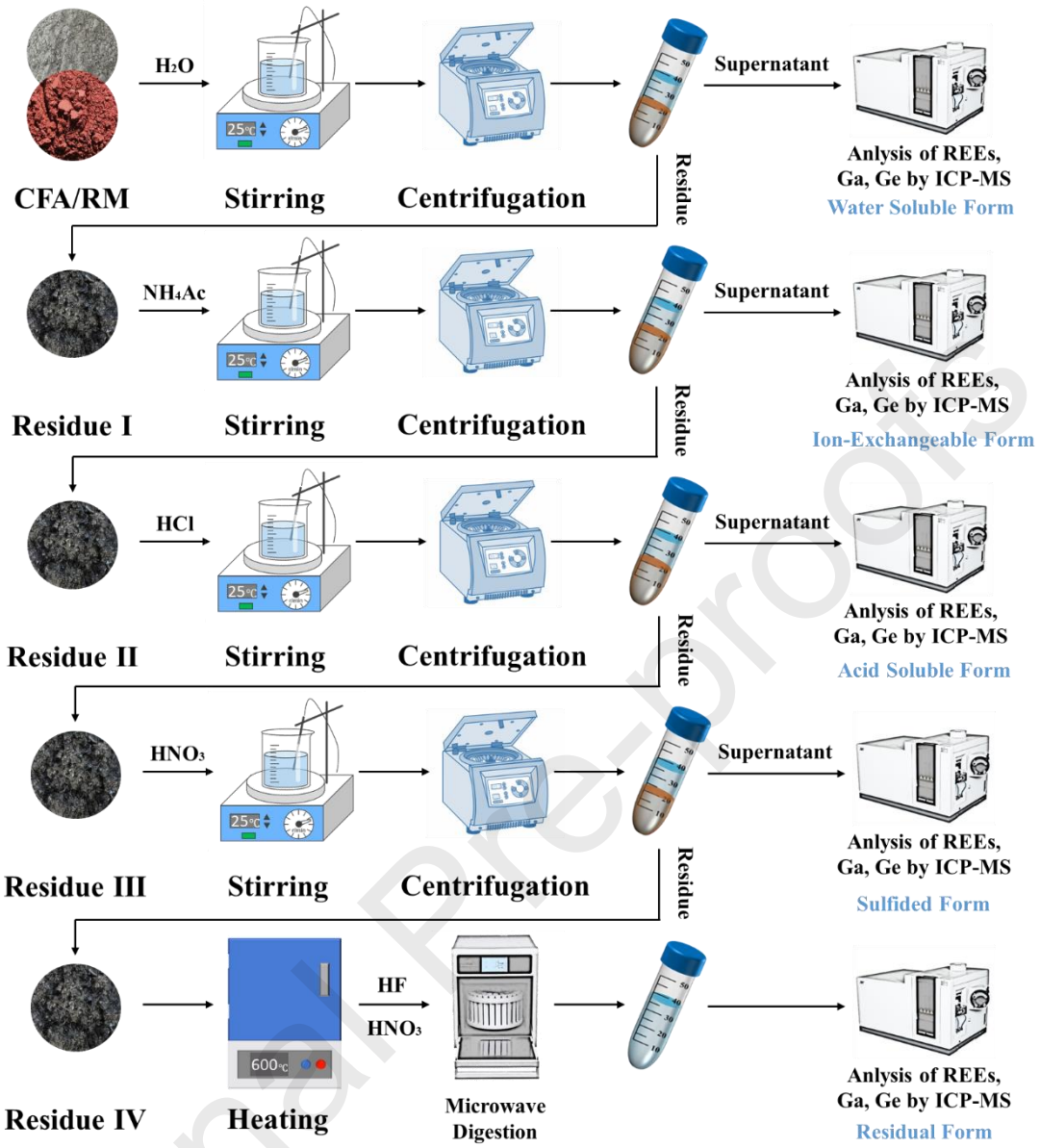

Figure 2. Schematic Diagram of Sequential Chemical Extraction

Table 2. Sequential Chemical Extraction Methods and Analytical Procedures

Step	Extraction Method	Sample	Further	Result
I	Weigh 1.00 g of sample, add 20 mL DI water and stir at 100 rpm for 24 h at RT;	Supernatant	ICP-MS analysis of REEs, Ga & Ge	WSF content of REEs, Ga & Ge
	Centrifuge at 10,000 rpm for 5 min.	Residue	Washing by DI	Residue I→Step

			water	II
II	Residue I, add 20 mL 1M NH_4Ac and stir at 100 rpm for 24 h at RT; Centrifuge at 10,000 rpm for 5 min.	Supernatant	ICP-MS analysis of REEs, Ga & Ge	IEF content of REEs, Ga & Ge
		Residue	Washing by DI water	Residue II→Step III
III	Residue II, add 20 mL 6M HCl and stir at 100 rpm for 24 h at RT; Centrifuge at 10,000 rpm for 5 min.	Supernatant	ICP-MS analysis of REEs, Ga & Ge	ASF content of REEs, Ga & Ge
		Residue	Washing by DI water	Residue III→Step IV
IV	Residue III, add 20 mL 2M HNO_3 and stir at 100 rpm for 24 h at RT; Centrifuge at 10,000 rpm for 5 min.	Supernatant	ICP-MS analysis of REEs, Ga & Ge	SF content of REEs, Ga & Ge
		Residue	Washing by DI water	Residue IV→Step V
V	Weigh 0.20 g of Residue IV, and heat at 600℃ for 1h; add 2 mL HF, 5 mL HNO_3 and microwave digestion for 10 min	Dilute	ICP-MS analysis of REEs, Ga & Ge	RF content of REEs, Ga & Ge

2.6 Alkali fusion-leaching activation process

The alkali fusion-leaching activation process disrupts the stable chemical structure of raw ores, converting insoluble mineral phases into readily extractable forms. Disintegrated silico-aluminum frameworks are subsequently removed via alkaline washing, reducing acid consumption during subsequent leaching and enhancing recovery efficiencies for REEs, Ga, and Ge.

Fly ash was mixed with sodium carbonate at a 1:1 silicon-to-aluminum molar ratio.

A 1 g portion of the mixture was placed in a crucible and heated in a muffle furnace to 860℃, maintained for 1 hour to complete the activation reaction. After cooling to room temperature, the calcined product was ground into a fine powder. Unlike fly ash, red mud required no prior calcination and was directly subjected to alkaline washing.

Subsequently, processed sample was mixed with a 20% (w/v) sodium hydroxide solution at a liquid-solid ratio of 20:1 (mL/g). Two sequential washes were performed at 60℃ for 30 minutes each, with continuous stirring to ensure homogeneity. Following filtration to separate the alkaline solution, the residual solid was reserved for acid leaching to recover REEs, Ga, and Ge.

2.7 Acid leaching experiment

Nitric acid exhibits superior dissolution capacity compared to hydrochloric acid, capable of decomposing nearly all speciation forms, including minor residual fractions, and achieving optimal acid leaching efficiency. Following ultra-fast FJH activation and subsequent alkali washing of fly ash and red mud samples, leaching experiments for REEs, Ga, and Ge were conducted using 1 M nitric acid as the leaching agent. The nitric acid solution was added to the activated solids at a liquid-solid ratio of 20:1 (mL/g), magnetically stirred for 60 minutes, and filtered. The filtrate was collected for analysis after settling to ensure particle-free supernatant.

2.8 Analytical Methods

The microwave digestion method was employed to decompose solid fly ash and red mud samples. Inductively coupled plasma mass spectrometer (ICP-MS) enables elemental analysis by ionizing samples via inductively coupled plasma, separating ions based on mass-to-charge ratio (m/z) through quadrupole mass spectrometry, and performing quantitative detection, achieving high-sensitivity simultaneous multi-element analysis [24]. Owing to its capability for accurate multi-element detection without prior separation, this technique was selected for analyzing REEs, Ga, and Ge in the sample, calculate their leaching recovery efficiencies from fly ash and red mud. The formula for calculating the leaching efficiencies of individual REEs, Ga, and Ge is provided in Equation 1, while the calculation for total REEs is presented in Equation 2.

$$\eta = \frac{C*V*k}{m*M} * 100\% \quad (1)$$

$$\eta = \frac{\sum(C_i*V*k)}{\sum(m*M_i)} * 100\% \quad (2)$$

η – Leaching efficiency of the element in the sample, Unit: %;

C – Element concentration in the leachate measured by ICP-MS, Unit: ng/mL;

C_i – the i-th REEs concentration in the leachate measured by ICP-MS, Unit: ng/mL;

V – Volume of the leachate, Unit: mL;

K – Dilution factor of the solution during measurement.

m – Mass of the sample, Unit: g;

M – Element mass concentration in the sample (Table 1), Unit: μg/g;

M_i – the i-th REEs mass concentration in the sample (Table 1), Unit: μg/g;

Additionally, a combination of X-ray diffractometer (XRD), X-ray photoelectron spectrometer (XPS), and scanning electron microscope (SEM) characterized the fly ash and red mud samples after FJH, calcination, and alkali washing treatments.

3. Results and Discussion

3.1 Structural changes of samples activated by different activation methods

Figure 3 illustrates the morphological and color changes of fly ash and red mud samples before and after the FJH process. Figure 3a presents a visual comparison of fly ash samples before and after the Joule heating experiment. The left image depicts a 2:1 fly ash-graphite mixture after ball milling, showing the original ash with its characteristic texture and light color. In contrast, the right image displays the activated sample post-Joule heating, which exhibits a notable transformation: the material darkens significantly, becomes more lustrous, and forms clumped structures. These observable changes indicate substantial morphological alterations in fly ash, suggesting that Joule heating caused the decomposition of aluminum- and silicon-containing compounds within the fly ash matrix. Figure 3b compares red mud samples before and after Joule heating. The pre-treatment sample (left image), a 2:1 red mud-graphite mixture after ball milling, retains the original reddish-brown hue typical of red mud. The post-treatment sample (right image), however, transitions to a dark reddish-black color, accompanied by distinct morphological changes. It can be seen that the morphology of the red mud has undergone significant changes. Thus concluded that the compounds of iron, aluminum, and silicon elements in red mud were broken by Joule heating.

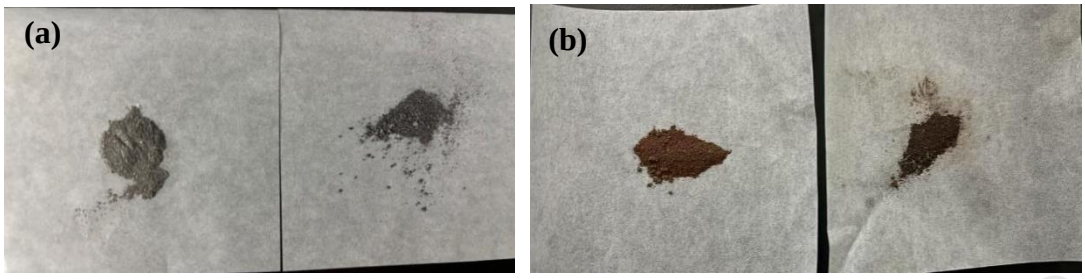

Figure 3. Images of the sample before and after activation. (a) Comparison of fly ash samples before and after FJH process, (b) Comparison diagram of red mud sample before and after FJH process

To characterize the black substance formed in the reacted red mud, a magnet response characteristics and XRD test was conducted, as shown in Figure 4. Before the experiment (Figure 4a), the red mud sample appeared as reddish-brown red mud, primarily composed of Fe_2O_3 with non-magnetic. As shown in Figure a, the sample was not attracted by the magnet. The reddish-brown color and non-magnetic behavior confirm that the sample mainly consists of iron oxide, which typically exhibits this color and lacks magnetism.

However, after FJH experiment(Figure 4b), color of the sample changed from reddish-brown to metallic silver-gray, indicating a significant transformation in its chemical composition. Figure b demonstrates that the treated sample became attracted to the magnet, suggesting the formation of magnetic Fe or other magnetic iron compounds (e.g., iron oxides or alloys) in the processed material.

The XRD patterns further confirm this conclusion. The XRD spectra in Figure 4c reveal distinct changes in the crystalline structure of the sample before and after the experiment. In the pre-experiment sample, the XRD pattern displays characteristic peaks of Fe_2O_3, consistent with the primary composition of the red mud.

In contrast, the post-experiment sample exhibits new characteristic peaks in its XRD pattern, which match those of metallic iron (Fe). These results suggest that Fe_2O_3 was reduced to iron or magnetic iron compounds (e.g., oxides or alloys) during the FJH treatment, thereby altering both the magnetic properties and color of the material..

These findings highlight a potential new pathway for efficient iron recovery from red mud through Joule heating-induced reduction reactions.

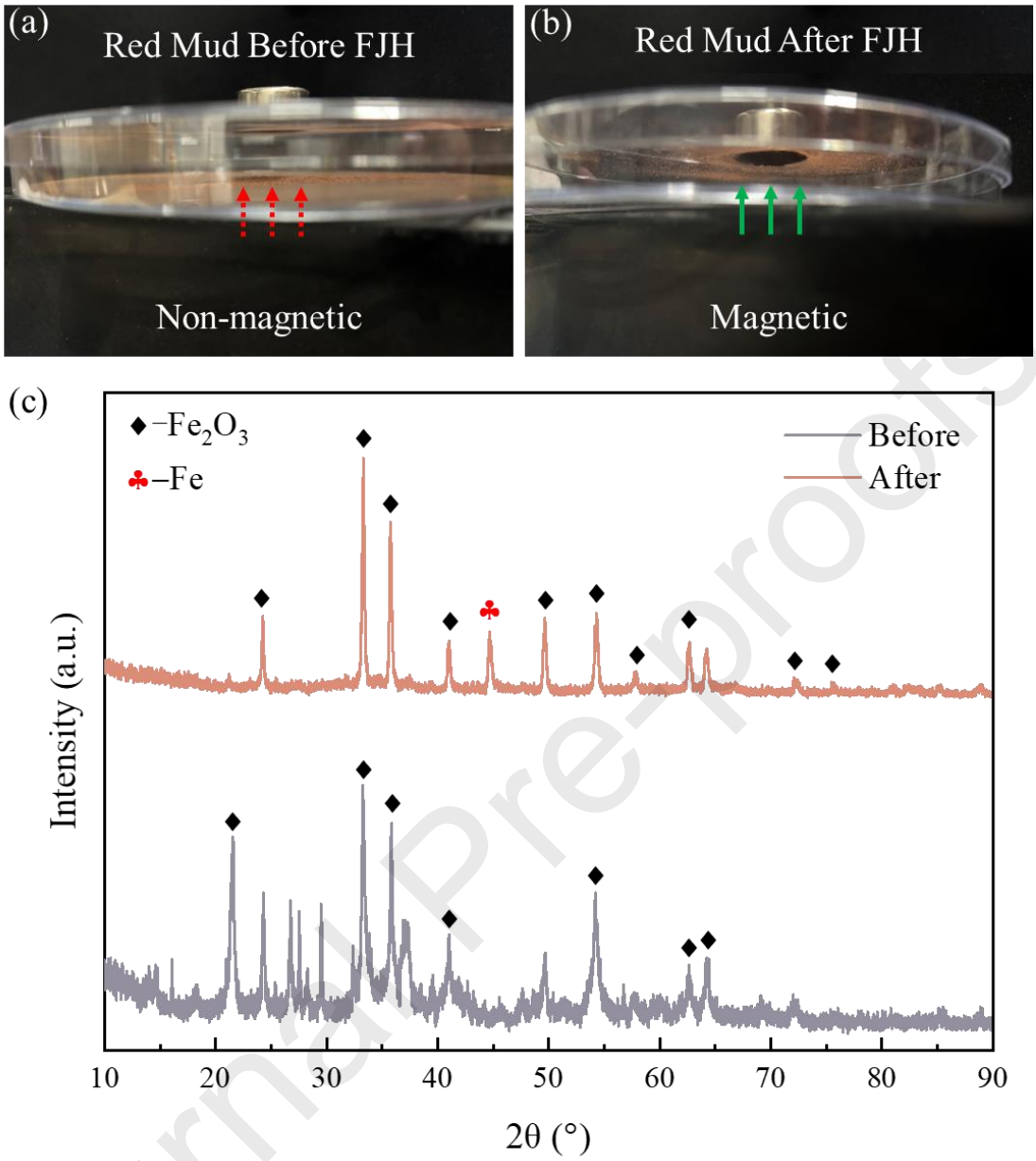

Figure 4. Magnetic response characteristics (a & b) and XRD patterns (c) of red mud before and after the FJH experiment.

Mineral analysis of the original fly ash and red mud samples, as well as the activated samples subjected to FJH and alkali-fusion alkali-leaching, was conducted using XRD to explore the phase transformations occurring before and after activation. As depicted in Figure 5a, following the ultra-fast FJH process, the fly ash exhibited no significant species alteration, with only diffraction peaks associated with conductive graphite detected at 43.6° and 45.1° [25]. This can be attributed to the use of graphite as a conductive agent during Joule heating. However, the peak of SiO_2 in the activated

sample was notably enhanced, while the peak of $3Al_2O_3{\cdot}2SiO_2$ was significantly diminished. This suggests that the aluminosilicates in fly ash underwent recrystallization or phase transformation under high-temperature conditions, resulting in a more ordered crystalline structure. After calcination and activation with additives, the internal structure of fly ash underwent substantial changes, with the diffraction peak corresponding to $3Al_2O_3{\cdot}2SiO_2$ in the range of 10-30° entirely disappearing. This indicates that the glassy matrix of fly ash, unburned carbon particles, and other amorphous oxides reacted with the activator at high temperatures. Post-activation, the original mullite almost entirely vanished, giving rise to various sodium-containing mineral phases, such as sodium silicate. This also implies that REEs, Ga, and germanium were liberated from the constraints of silicon and aluminum, creating favorable conditions for their subsequent extraction and utilization. As shown in Figure 5b, red mud primarily consists of hematite, alumina, and silica. After undergoing the ultra-fast FJH process, the red mud sample experienced significant phase changes. The iron oxide peaks at 30° and 35° were markedly enhanced, indicating an increase in the crystallinity of hematite. Additionally, the Joule heating process led to the formation of magnetite, suggesting that iron oxide underwent a reduction reaction with conductive graphite at high temperatures. This explains why red mud samples become magnetic after Joule heating activation. Compared to red mud, following the alkali-leaching experiment, the sample's diffraction peak was significantly weakened, with hematite and alumina undergoing conversion or dissolution between 30°-40°. Furthermore, a new peak of Na_2SiO_5 emerged post-reaction, revealing the generation of sodium silicate during alkali leaching and the decomposition of the silicon structure in red mud. To further confirm the changes in the Al-Si-O phases, we conducted XPS analysis. XPS characterization further verified the alterations in Al-Si-O, as shown in Figures S1 and S2 included in the supplementary materials.

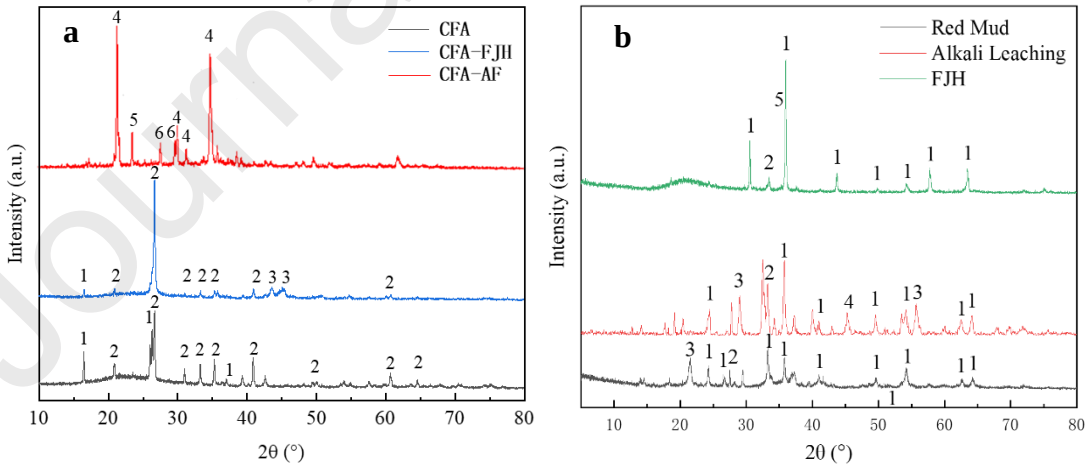

Figure 5. XRD patterns of the sample before and after activation.

(a) Comparison of fly ash samples before and after activation (1-3-$Al_2O_3{\cdot}2SiO_2$, 2-SiO_2, 3-Graphite, 4-$NaAlO_2$, 5-$NaAlSiO_4$, 6-Na_2SiO_3), (b) Comparison of red mud samples before

and after activation (1-Fe_2O_3, 2-Al_2O_3, 3-SiO_2, 4-Na_2SiO_5, 5-Fe_3O_4)

The original samples of fly ash and red mud and the samples activated by FJH and alkali-fusion alkali-leaching were characterized using SEM to study the changes in internal structure before and after activation. Figure 6a shows the morphology of untreated fly ash, with particles in a ball-like shape. Figure 6b shows that after the FJH process, the microstructure of fly ash undergoes significant changes, with particles exhibiting different pore structures, especially in smaller particle sizes where pores become larger or more pronounced, and small cracks or voids may appear on the surface.

As observed in Figure 6c, the original large block structure and the portion supporting the silicon aluminum structure entirely disappeared from the fly ash treated with alkali-fusion alkali-leaching. Figure 6d shows the microstructure of red mud, with irregular particle shapes and varying sizes, some of which were blocky or fragmented, and obvious pore structures, indicating that its mineral composition contains many porous substances (such as iron ore, bauxite, etc.). The surface morphology of red mud undergoes significant changes following the FJH process, as seen in Figure 6e. The surface becomes smoother, the pore structure is more uniform, the particle boundaries are more distinct, and the pore structure exhibits larger porosity and higher orderliness. Figure 6f shows that the alkaline washing process significantly improves red mud's surface morphology and pore structure, making the particle surface smoother, reducing agglomeration, optimizing the pore structure, making the surface more uniform, and exposing more active sites. Overall, the two activation treatment methods significantly altered the surface structure of fly ash and red mud, resulting in high porosity and exposure of more active sites, facilitating acid permeation through the pores and improving the extraction efficiency of REEs, Ga, and Ge.

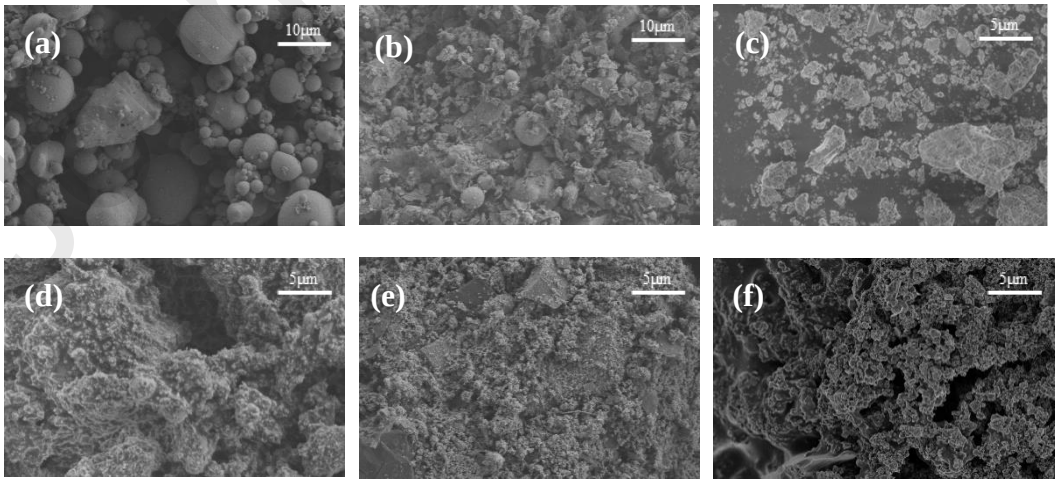

Figure 6. SEM images of samples before and after activation.

(a) Original sample of fly ash, (b) activated by Joule heating of fly ash, (c) activated by calcination-alkali washing of fly ash. (d) Original red mud sample, (e) activated by Joule heating of red mud, (f) activated by calcination-alkali washing of red mud sample

3.2 Speciation Evolution of REEs, Ga, and Ge via different activation methods

Following sample activation, the speciation of REEs, Ga, and Ge was characterized via ICP-MS analysis. Figure 7a shows how the speciation of REEs change in untreated fly ash samples under FJH at different voltages, compared with additive calcination treatment. As the Joule heating voltage increases, the combined proportion of acid-soluble, ion-exchangeable, and sulfurized form REEs fractions rises sharply. This trend coincides with the decomposition of aluminosilicate structures, and the total reaches nearly 90%. This indicates that FJH effectively converts REEs encapsulated in the lattice into leachable forms. The changes in the speciation of REEs in red mud before and after various activations are illustrated in Figure 7b. In accordance with the fly ash sample, the REEs found in the primary constituents of red mud are more prone to leaching, resulting in a significant quantity of residual REEs being converted into acid-soluble forms. Joule heating activation reaches or approaches the level after auxiliary roasting treatment, providing favorable support for subsequent REEs recovery and extraction and expanding production. Figures 7c and 7d show the occurrence characteristics of Ga in fly ash and red mud after activation. After the FJH treatment, the easily extractable form of Ga gradually increased from 20% to about 70% with the voltage increase. Although slightly inferior to the alkali washing activation treatment, the proportion of easily extractable forms increased significantly. The ultra-fast FJH activation approach altered the morphology of Ga, and further physical and chemical auxiliary techniques can enhance the recovery and extraction efficiency of Ga. Figures 7e and 7f show the changes in the forms of Ge in fly ash and red mud after different activation schemes, respectively. After the FJH activation treatment, Ge's original water-soluble and acid-soluble structures were decomposed and transformed into residual form. However, with increased FJH voltage and temperature, Ge changed from residual form to easily extractable form. The ultra-fast FJH activation treatment significantly influences the distribution of REEs, Ga, and Ge in fly ash and red mud, enhancing the acid-soluble fraction while diminishing the residual fraction. This reduced the complexity of later extraction of REEs and enhanced recovery and extraction efficiency.

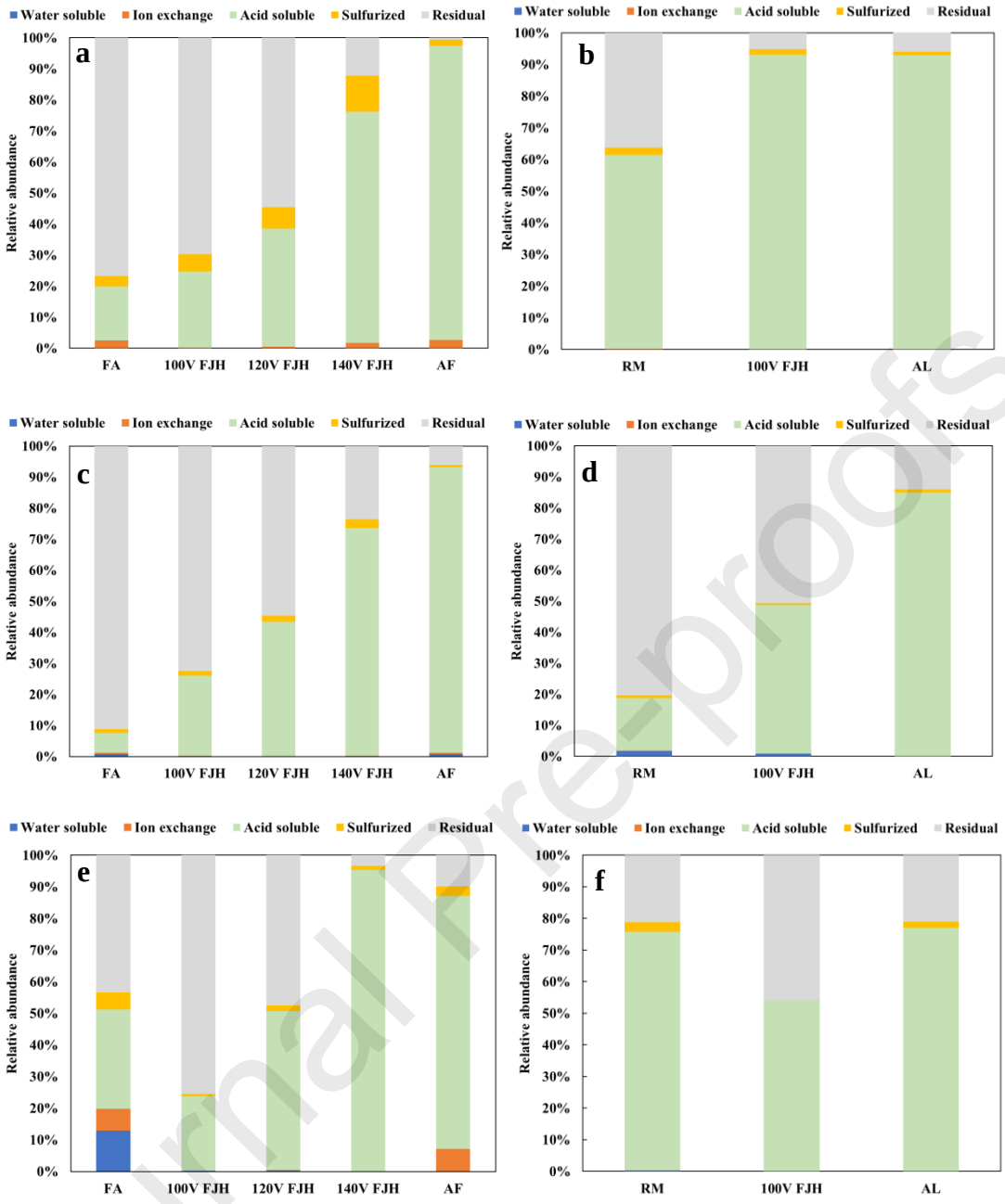

Figure 7. Distribution of speciation before and after sample activation.

REEs in (a) fly ash and (b) red mud, Ga elements in (c) fly ash and (d) red mud, and Ge in (e) fly ash and (f) red mud

3.3 Comparison and analysis of recovery and extraction efficiency by different methods

Following various activation methods, the REEs, Ga, and Ge in fly ash and red mud were anticipated to be efficiently concentrated through acid-leaching extraction.

The recovery and extraction efficiency of REEs, Ga, and Ge in samples subjected to flash evaporation and Joule heating at varying voltages were analyzed. To evaluate the recovery and extraction efficiency, alkaline pre-activation and direct acid dissolution without pre-treatment were set as upper and lower limits, respectively. Figure 8a illustrates that the effective current of the sample increases with voltage, and the temperature of the sample heated by FJH markedly increases. The wrapped silicon-aluminum structure endured a more substantial destructive force, releasing REEs, Ga, and Ge, enhancing acid-leaching recovery and extraction efficiency. The extraction efficiency of REEs exceeded 95%, while the efficiency of Ge was above 90%. In contrast, the extraction efficiency of Ga was relatively low, about 80%. As indicated in Figure 8b, the silicon-aluminum structure wrapped REEs, Ga, and Ge within the fly ash, existing in a residual form. Alkaline pre-activation and the FJH process can decompose the silicon-aluminum structure to diminish the residual form; however, direct acid dissolution is ineffective. Concurrently, an increased release of REEs, Ga, and Ge was observed due to the enhanced destructive capability of FJH, resulting in improved extraction efficiency.

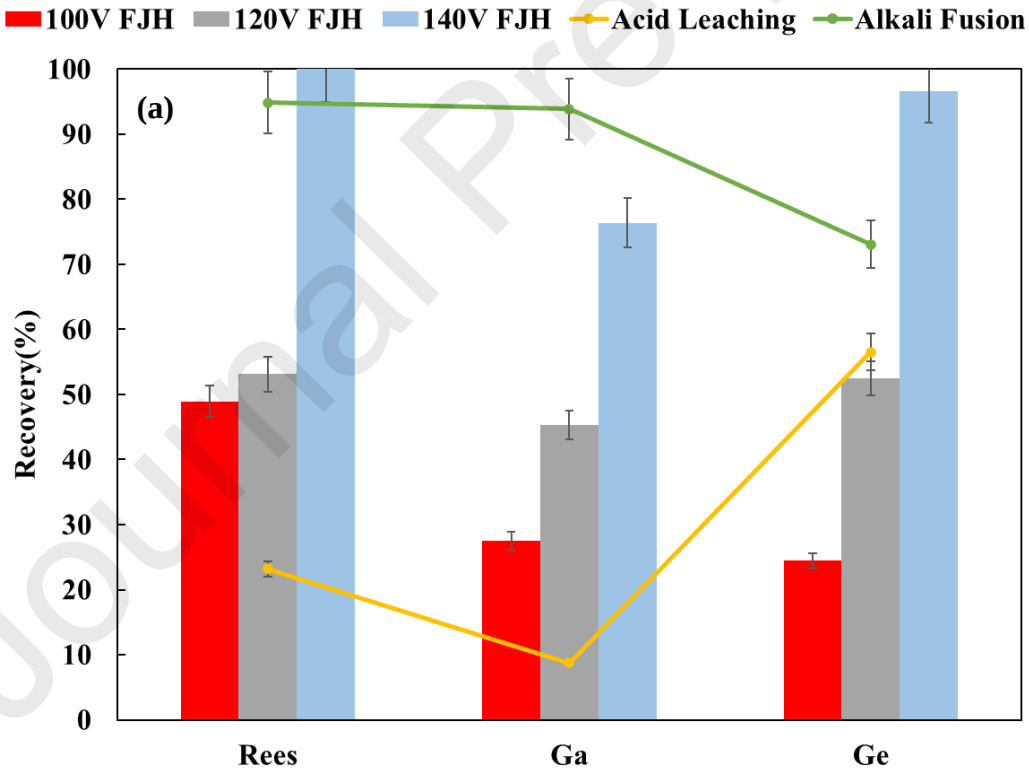

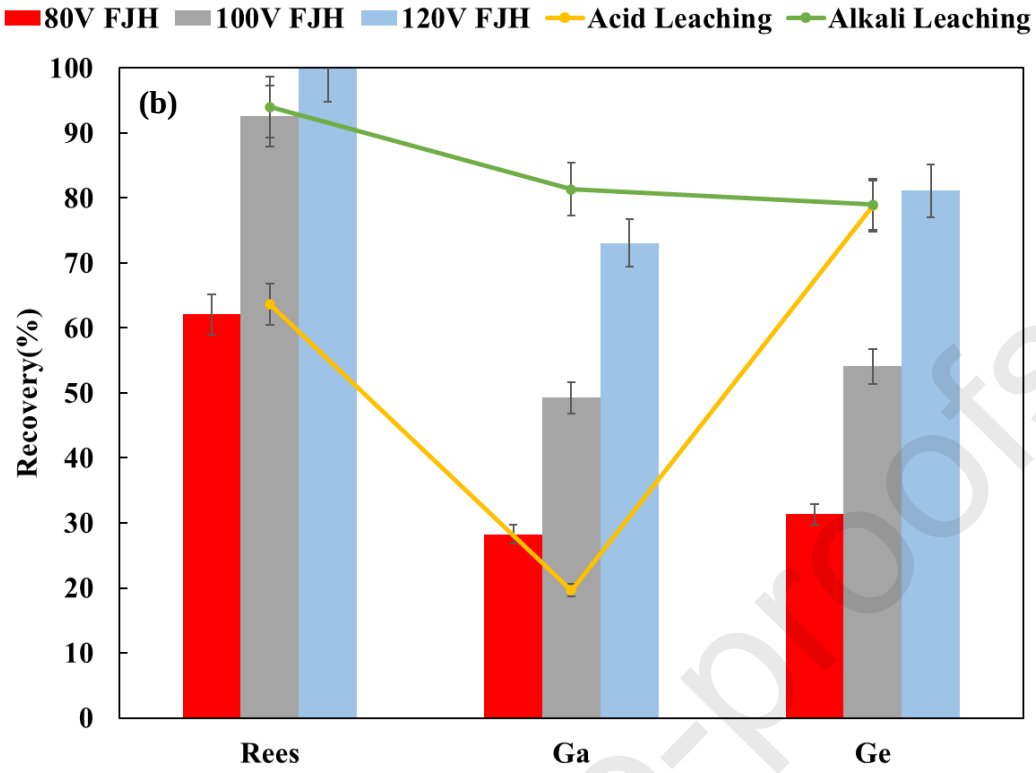

Figure 8. Extraction efficiency of REEs and scattered Ga, Ge before and after sample activation. (a) Extraction efficiency of fly ash and (b) red mud under different working conditions

3.4 Analysis of material and energy consumption by different activation methods

In the context of efficient separation and recovery of REEs, Ga, and Ge from fly ash or red mud, material and energy consumption are critical parameters alongside extraction efficiency, directly impacting cost-effectiveness, process scalability, and sustainability. Table 3 details the raw material and energy requirements for treating 1 kg of fly ash or red mud using the ultra-fast FJH activation method versus the alkali-fusion alkali-leaching approach. Notably, both processes utilize common chemicals, with relatively costly graphite and sodium hydroxide (NaOH) recyclable post-separation, further mitigating operational costs.

Under consistent acid leaching conditions, the FJH method requires only 0.5 kg of graphite powder and 1.68 kW·h of electricity (calculated at 120 V discharge), exemplifying its high-energy efficiency. In contrast, the alkali-fusion alkali-leaching process for fly ash involves two stages: it consumes 1.3 kg of sodium carbonate (Na_2CO_3), 8 kg of NaOH, and 6 kW·h of electricity (based on two cycles in a 2.5 kW furnace), with the alkali-fusion step dominating energy use. Red mud treatment via

alkali-leaching alone demands 8 kg of NaOH and 1 kW·h of energy. The FJH method reduces electricity consumption by two-thirds for the same material mass, simultaneously achieving energy savings and lowering greenhouse gas emissions.

The alkali-fusion process's high energy and Na_2CO_3 requirements highlight FJH's distinct advantages, particularly for fly ash. Additionally, FJH completes a single experiment in 1 minute or less, markedly faster than the prolonged heating/cooling cycles of alkali-leaching. However, current FJH technology is constrained by processing capacity, limiting short-term large-scale sample treatment, whereas alkali-fusion alkali-leaching is mature and easily scalable, with by-products like aerogel and white carbon black enhancing its economic value [26-27].

Notably, technological advancements have enabled the development of FJH devices capable of processing 100 tons of solid waste daily by 2024, though its annual capacity of 30,000 tons still lags behind industrial demands. Nonetheless, FJH's low-energy, low-emission, and low-material footprint underscores its transformative potential for future waste valorization. In practical applications, selecting recovery methods tailored to specific operational contexts, balancing economic viability and environmental sustainability, will be key to optimizing strategic element extraction from industrial waste streams.

Table 3. Energy consumption comparison of different activation methods

	FJH			AF-AL			
	FA & RM			FA		RM	
Step	Reagent/Energy	Amount	Step	Reagent/ Energy	Amount	Reagent	Amount
FJH	Graphite	0.5 kg	Alkali Fusion	Na_2CO_3	1.3 kg	--	--
				860 ℃ 1h	5 kW·h	--	--
	Flashing	1.68	Alkali	NaOH	8 kg	NaOH	8 kg

		kW·h	Leaching	60 ℃ 1h	1 kW·h	60 ℃ 1h	1kW.h
Acid Leaching	Nitric acid	1.25 L	Acid Leaching	Nitric acid	1.25 L	Nitric acid	1.25 L
	Stir 1 h	0.1 kW·h		Stir 1 h	0.1 kW·h	Stir 1 h	0.1 kW·h

4. Conclusions

This study introduces an ultra-fast FJH activation method combined with acid leaching for extracting REEs, Ga, and Ge from fly ash and red mud, contrasting it with the conventional alkali-fusion alkali-leaching approach. The FJH treatment generates intense Joule heating and material volatilization, disrupting the silicon-aluminum framework in fly ash while inducing reduction-transformation of iron oxides in red mud. These effects facilitate the conversion of lattice-encapsulated REEs in both matrices from residual, inert forms into acid-soluble form. Compared to direct acid leaching, this strategy markedly boosts REEs extraction efficiency, surpassing 90%, comparable to alkali-fusion methods, by breaking down the refractory silicate-aluminate structures. For Ga, FJH effectively transforms its residual phase into acid-soluble forms, enhancing recovery from fly ash and red mud; however, a 20–30% improvement potential remains relative to the theoretical maximum leaching rate. In the case of Ge, while initial FJH conditions temporarily convert its water/acid-soluble fractions into residual forms, increasing the applied voltage drives a secondary transformation of these residual species into acid-soluble states, ultimately achieving extraction rates that exceed those of Ga.

The FJH-acid leaching process efficiently extracts target elements from coal-based solid waste and red mud with minimal material and energy input, enabling cost-effective recovery of strategic critical elements. By enhancing waste resource utilization and promoting sustainable management of fly ash and red mud, this approach bridges the gap between environmental sustainability and economic viability in industrial waste valorization.

Declaration of Competing Interest

The authors declare no competing financial interest.

Acknowledgements

This work was supported by grants from the National Natural Science Foundation of China (Grant No. 22178339), 2023 Innovation-driven Development Special Foundation of Guangxi Province (AA23023021), the University Science Research Project of Anhui Province (2022AH050076), the Hundred Talents Program (A) of the Chinese Academy of Sciences.

Data availability

No data was used for the research described in the article.

Reference

1. Critical Mineral Resources of the United States-Economic and Environmental Geology and Prospects for Future Supply. 2017, Reston: U. S. Geological Survey.

2. National Mineral Resources Master Plan (2016-2020), T.M.o.l.a.r. P.R.C., Editor. 2016.

3. Yuwei, L., Research on strategic mineral resource inventory, supply-demand situation and countermeasures. Science & Technology Review, 2024. **42**(05): p. 26-37.

4. Research Report on the Development and Operation Status and Investment Strategy of China's Fly Ash Industry from 2024 to 2030 2204.11.13, Huaxia Industrial Economy Research Institute.

5. China, T.o.N.M.S.o., Breakthrough of 10 million tons-Significant progress made in green utilization of red mud in China in 2023. 2024. 01.05.

6. Zhang Lei, Chen Hangchao, and P. Jinhe, Research progress on occurrence characteristics, enrichment and extraction of coal-based lithium and rare earth Conservation and Utilization of Mineral Resources, 2023. **43**(6): p. 1-13.

7. Liu, Y. and R. Naidu, Hidden values in bauxite residue (red mud): Recovery of metals. Waste Management, 2014. **34**(12): p. 2662-2673.

8. Li Hailan, Zhang Jie, and W. lin, REE resources in red mud: distribution, occurrence and extraction. Acta Mineralogica Sinica, 2021. **41**(Z1): p. 578-592.

9. Blissett, R.S., N. Smalley, and N.A. Rowson, An investigation into six coal fly ashes from the United Kingdom and Poland to evaluate rare earth element content. Fuel, 2014. **119**: p. 236-239.

10. Lin, R., et al., Enrichment of rare earth elements from coal and coal by-products by physical separations. Fuel, 2017. **200**: p. 506-520.

11. Stojković, M., et al., Recovery of Rare Earth Elements from Coal Fly and Bottom Ashes by Ultrasonic Roasting Followed by Microwave Leaching. Metals, 2024. **14**(4): p. 371.

12. Pan, J., et al., Recovery of rare earth elements from coal fly ash through sequential chemical roasting, water leaching, and acid leaching processes. Journal of Cleaner Production, 2021. **284**: p. 124725.

13. Taggart, R.K., J.C. Hower, and H. Hsu-Kim, Effects of roasting additives and leaching parameters on the extraction of rare earth elements from coal fly ash. International Journal of Coal Geology, 2018. **196**: p. 106-114.

14. Mokoena, B.K., L.S. Mokhahlane, and S. Clarke, Effects of acid concentration on the recovery of rare earth elements from coal fly ash. International Journal of Coal Geology, 2022. **259**: p. 104037.

15. Algozeeb, W.A., et al., Flash Graphene from Plastic Waste. ACS Nano, 2020. **14**(11): p. 15595-15604.

16. Advincula, P.A., et al., Flash graphene from rubber waste. Carbon, 2021. **178**: p. 649-656.

17. Wyss, K.M., et al., Upcycling end-of-life vehicle waste plastic into flash graphene. Communications Engineering, 2022. **1**(1): p. 3.

18. Yin, Y.-C., et al., Rapid, Direct Regeneration of Spent $LiCoO_2$ Cathodes for Li-Ion Batteries. ACS Energy Letters, 2023. **8**(7): p. 3005-3012.

19. Guo, C., et al., Light-induced quinone conformation of polymer donors toward 19.9% efficiency organic solar cells. Energy & Environmental Science, 2024. **17**(7): p. 2492-2499.

20. Chen, W., et al., Flash Recycling of Graphite Anodes. Advanced Materials,

2023. **35**(8): p. 2207303.

21. Qian, F., et al., Asymmetric active sites originate from high-entropy metal selenides by joule heating to boost electrocatalytic water oxidation. Joule, 2024. **8**(8): p. 2342-2356.

22. Zhu, X.H., et al., Recycling Valuable Metals from Spent Lithium-Ion Batteries Using Carbothermal Shock Method. Angew Chem Int Ed Engl, 2023. **62**(15): p. e202300074.

23. Deng, B., et al., Heavy metal removal from coal fly ash for low carbon footprint cement. Communications Engineering, 2023. **2**(1): p. 13.

24. Beauchemin, D. Inductively coupled plasma mass spectrometry. Analytical Chemistry, 2008. **80**(12): p.4455.

25. Deng, B., et al., Rare earth elements from waste. Science Advances, 2022. **8**(6): p. 3132.

26. Zhang, L., et al., A study on preparation and properties of fly ash-based SiO2 aerogel material. Colloids and Surfaces A: Physicochemical and Engineering Aspects, 2024, 684: p. 133016.

27. Liu, D. D., et al., Preparation of White Carbon Black from Fly Ash Modified with Silane Coupling Agents and Its Dispersion Properties. Fine Chemicals, 2019, **36**(4): p. 588.

Highlights

1. Rare earth elements, Gallium and Germanium were recovered from fly ash and red mud.
2. Ultra-fast Flash Joule Heating (FJH) method was attractive in element recovery.
3. FJH method exhibited low energy and acid consumption without alkali involvement.
4. The acid leaching efficiency after FJH pretreatment exceeded 80%.